Photonics and Nanostructures - Fundamentals and Applications 52 (2022) 101075

Contents lists available at ScienceDirect

Photonics and Nanostructures - Fundamentals and Applications

journal homepage: www.elsevier.com/locate/photonics

Versatile optical beam routers based on inversely designed supercell metagratings

Xixian Zu [a,b,c], Boqu Chen [b,c], Ni Tang [b,c], Wei E.I. Sha [d], Jiyong Wang [b,c,*], Min Qiu [b,c,*]

[a] State Key Laboratory of Modern Optical Instrumentation, College of Optical Science and Engineering, Zhejiang University, Hangzhou 310027, PR China
[b] Key Laboratory of 3D Micro/Nano Fabrication and Characterization of Zhejiang Province, School of Engineering, Westlake University, 18 Shilongshan Road, Hangzhou 310024, Zhejiang Province, PR China
[c] Institute of Advanced Technology, Westlake Institute for Advanced Study, 18 Shilongshan Road, Hangzhou 310024, Zhejiang Province, PR China
[d] College of Information Science and Electronic Engineering, Zhejiang University, Hangzhou 310027, PR China

ARTICLE INFO

Keywords:
Diffractive optical elements
Supercell metagrating
Inverse design
Beam routing
Rigorous coupled-wave analysis

ABSTRACT

Metagratings manipulating the wavefront with a subwavelength volume have been widely explored in recent years for their potential applications in optical beam routers, such as laser beam splitters and combiners. Current metagratings are hampered from practical beam rerouting due to inhibitive computational load of engineering design and expensive nanofabrication cost. In this work, we apply the emerging concept of supercell metagratings, which arranges random binary gratings of a unit cell in a one-dimensional periodicity, to simplify such design and fabrication processes. A high-performance inverse design framework for the supercell gratings is proposed. In such a framework, we use coupled wave algorithm as a fast-converging electromagnetic solver for the forward calculation and particle swarm optimization algorithm for the backward optimization. By manipulating the building blocks of a unit cell, specific diffraction orders of supercell gratings can be intentionally strengthened or eliminated. We finally realize high-efficiency, broadband and multi-functionality optical beam splitters and combiners both in visible and near-infrared regimes. We envision that the proposed method offers an avenue towards the mass production realization of flat optics.

1. Introduction

Conventional optical waveshaping is realized through geometrical optics elements, such as converging/diverging lens, transflective cubes, prisms, polarizers, waveplates and spatial light modulators [1]. The wavefront of the propagating beam is manipulated in a medium much thicker than the wavelength, giving rise to a bulky and large-scale optical system. Metasurfaces are artificial two-dimension (2D) sheets that repeat the unit cells in a subwavelength array [2–5]. The amplitude and phase distribution of the light can be tuned by the spatial distribution and orientation of the unit cell. Such properties have paved the way toward the concept of flat optics, including the flat lenses [6], polarizers [7,8], holograms [9], and collimators [10,11] to name a few. Contrast to bulk geometric elements, metasurfaces manipulate the wavefront with a subwavelength volume.

Inspired by metasurfaces, metagratings are periodic arrays of nanostructures that enable highly-efficient wave transformation which is inaccessible using randomly arranged metasurfaces [12–19]. 1D metagratings, also conventionally termed as supercell gratings, have been proposed to further simplify the nanofabrication processes and promote the multi-order diffraction efficiencies [20]. A supercell grating is composed of periodic unit cells in one direction. Inside of each unit cell, there are lamellar gratings organized in a random manner. If the width resolution of lamellar gratings is regarded as a digital 'bit', the unit cell turns to be a binarized 'byte' data structure. By engineering the grating depth, the 'byte' dimension, the 'bit' resolution and their sequences inside a 'byte', one can obtain radiation nulls in the directions of all diffraction orders except the desired one [21–23]. Owing to the advantages of simple nanofabrication and limited number of design parameters, supercell metagrating has been widely applied in antenna performance enhancement [24], perfect absorbers [25], metalenses [26–28], energy harvesting [29] and optical beam rerouting [30].

Abbreviations: DOE, RCWA.

* Corresponding authors at: Key Laboratory of 3D Micro/Nano Fabrication and Characterization of Zhejiang Province, School of Engineering, Westlake University, 18 Shilongshan Road, Hangzhou 310024, Zhejiang Province, PR China.
E-mail addresses: wangjiyong@westlake.edu.cn (J. Wang), qiumin@westlake.edu.cn (M. Qiu).

https://doi.org/10.1016/j.photonics.2022.101075
Received 31 July 2022; Received in revised form 20 September 2022; Accepted 21 September 2022
Available online 24 September 2022

Despite of their advantages, supercell metagratings suffer from limited performance and low efficiency if multifunctionality of wave-shaping is needed, due to the neglects of near- and far-field interactions caused by optical coupling between different 'bits' [31]. Most of the current work adopts traditional 'effective index-phase gradient' concept, which relies on sweeping and manually adjusting geometry parameters of supercell gratings, in order to achieve required phase accumulations. The process is time-consuming and the output device tends to have a single functionality and poor reliability. Taking supercell-based beam splitter as an example, most of the work reported so far can only achieve energy splitting for a fixed-polarized light [22]. Few studies have been reported to quantitatively manipulate the energy ratio and the uniformity of each route of incident beams with arbitrary polarizations. The multifunctional high-efficiency beam splitters and combiners are desired in photonic integration due to the flexible and diversified capability of controlling the flow of light [32,33].

Here, we introduce the inverse design concept to help the design of supercell-based optical beam routers. We propose a new inverse design framework that quantitatively tailors efficiencies of expected diffraction orders. Instead of using 'effective index-phase gradient' method and brute-force parameter sweeping, we use coupled wave algorithm as an electromagnetic solver for the forward calculation and introduce particle swarm optimization algorithm to the backward optimization. By ingeniously defining the objective cost function, we can optimize the structural geometry and obtain multifunctional devices for two orthogonal polarizations simultaneously. This proposed framework is featured by high-efficiency, flexibility, and multi-functionality. As proof of concepts, we demonstrate the excellent performances of supercell metagratings to split and combine the optical beams in the both visible and near-infrared regimes.

2. Methods

A typical layer structure of the supercell metagrating is shown in Fig. 1(a), comprising a substrate, optional one or more intermediate uniform slabs, a grating layer and a superstrate. The grating has a long-range periodicity. In each period, the lamellar gratings are organized to a digital 'byte', which is formed by N 'bits'. The bit '1' means the groove material keeps the same as the grating ridges, while the bit '0' means it has the identical material as the superstrate. To achieve the expected waveshaping, both the material and geometric parameters should be carefully selected. Considering the large byte dimension N and sufficient targeting parameters, conventional methods relying on repeated sweeping can be time-consuming.

To improve the computational efficiency and accuracy, we propose here a multi-objective optimization-based inverse design framework, consisting of a forward electromagnetic (EM) solver, a backward multi-objective optimizer and a sensitivity analyzer, as depicted in Fig. 1(b). The forward EM solver is carried out through coupled wave method, or conventionally called rigorous coupled-wave analysis (RCWA) [34,35]. RCWA is a semi-analytical method to calculate the EM field and diffraction efficiencies of periodic structures, which shows outstanding converging rate for large-scale computations without losing the accuracy [36,37]. By using proper factorizations and truncations, we reformulate and expand conventional RCWA to conical diffractions and cascaded multilayers [38–40]. The enhanced EM solver is applicable to both dielectric and metallic grating materials with high numerical stability and fast converging rate (see the details from 'Supplemental

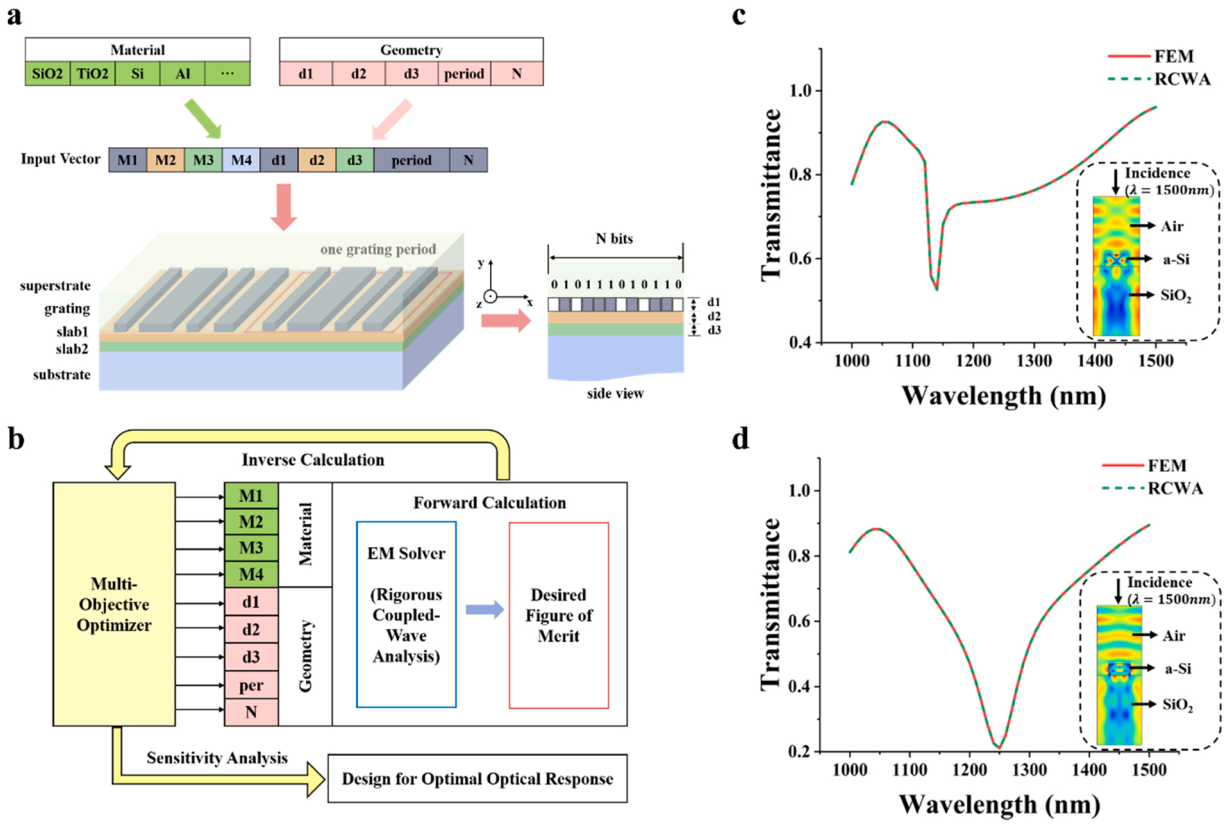

Fig. 1. Computational framework and EM solver benchmark of metagrating-based inverse design. (a) The layer structure of a multifunctional supercell metagrating device. (b) The computational framework for the inverse design of supercell metagrating, mainly including a forward EM solver, a backward multi-objective optimizer and a sensitivity analyzer. (c) Transmittance of a 1D binary grating calculated by using coupled-wave method (green dashed line) and finite-element method (red solid line). The incident beam is TE polarized. The inset shows the electric field distribution with an incident wavelength of 1500 nm. (d) Transmittance of a 1D binary grating calculated by using coupled-wave method (green dashed line) and finite-element method (red solid line). The incident beam is TM polarized. The inset shows the electric field distribution with an incident wavelength of 1500 nm.

Documents'). As shown in Fig. 1(c,d), we compare the total transmission efficiencies calculated by RCWA with commercially available finite-element software (COMSOL Multiphysics version 5.6) for transverse-electric (TE) and transverse-magnetic (TM) plane-wave incidences, respectively. The benchmark model is a lamellar grating, using SiO_2 as substrate and amorphous-silicon (a-Si) as grating material (see the details of material properties from 'Supplemental Document'). The light is normal incident from the air. The grating is periodic in *x* axis and invariant in *z* axis. The period is 1.3 times of the wavelength. The grating depth is 500 nm and the filling factor is 0.5. The insets in Fig. 1(c) and Fig. 1(d) show the electric field distributions ($|E|$) in *xy*-plane with an incident wavelength of 1500 nm for TE and TM polarization, respectively. A remarkable consistence between the two EM solvers over a broad range of wavelengths (from 1000 nm to 1500 nm) can be observed. These results prove the accuracy of our RCWA program.

The backward optimizer can be executed by any intelligent evolutionary algorithms. In this work, we choose particle swarm optimization (PSO) algorithm. PSO is a non-gradient method, which seeks the optimal solution by moving the particles by varying the search positions and velocities [41]. The advantage of PSO is obvious, that is multi-dimension and global convergence. We used local sensitivity analysis as the sensitivity analyzer in this work [42]. The term local refers to the fact that all derivatives are taken at a single point. By comparing different partial derivatives, we can find the most significant parameter influencing the cost function.

3. Results and discussions

As proof of concepts, a variety of optical beam routers including two laser beam splitters working in different wavelength bands, and one laser beam combiner are designed by using the supercell metagratings and inverse design algorithms. Taking the uniformity and energy ratio of diffraction orders of diffractive optical elements (DOEs) into account, the following function is used as figure of merit (FoM) function during the optimization:

$$\mathrm{FoM} = \sum_{\lambda_i}\left\{\sum_{m=1}^{M}(\eta_m - \eta_{m\_obj})^2 + \sum_{n=1}^{N}(\eta_n - \eta_{n\_obj})^2\right\}$$

Where η_m/η_n represents the calculated diffraction efficiencies for different polarizations or different incident angles. $\eta_{m\_obj}/\eta_{n\_obj}$ represents the target diffraction efficiency for different polarizations or different incident angles. λ_i is the wavelength of incident light (see the details from 'Supplemental Documents').

For the laser beam splitters, as depicted in Fig. 2(a), we aim at dividing the incident beams into several energy-equal beams and allowing the maximal conversion efficiencies. We assume that light is normally incident in the air from the substrate side of the beam splitter. The beam splitter has polarization characteristics. For instance, if the light is TM polarized, the incident beam is divided into three beams. If the light is TE polarized, the incident beam is divided into two beams. This kind of beam splitter can facilitate the parallel fabrication in laser machining and scanning laser projections to expedite the laser working processes. However, most of beam splitters reported realized the beam separation for a fixed-polarized light [22]. When the polarization is changed, the uniformity of separated beams cannot be fully guaranteed.

In our case, we assume that the incident wavelength is 1240 nm and the activated diffraction orders are 0 and ± 2. The period of supercell gratings is bounded between 2λ and 3λ to guarantee sufficient high diffraction efficiencies in ± 2 orders. The grating ridge material we choose is amorphous Si, and the substrate is SiO_2. The geometric parameters to be optimized include the grating depth, the 'bit' resolution, the 'byte' dimension and the binary sequence.

For the TE polarization, as can be seen from the far-field (500 μm away from the beam splitter, see the details from 'Supplemental Documents') electric intensity distributions in Fig. 2(b), the incident light is divided into two energy-equal beams. The diffraction orders of the beams are ± 2, while the zero order is entirely depressed. For the TM

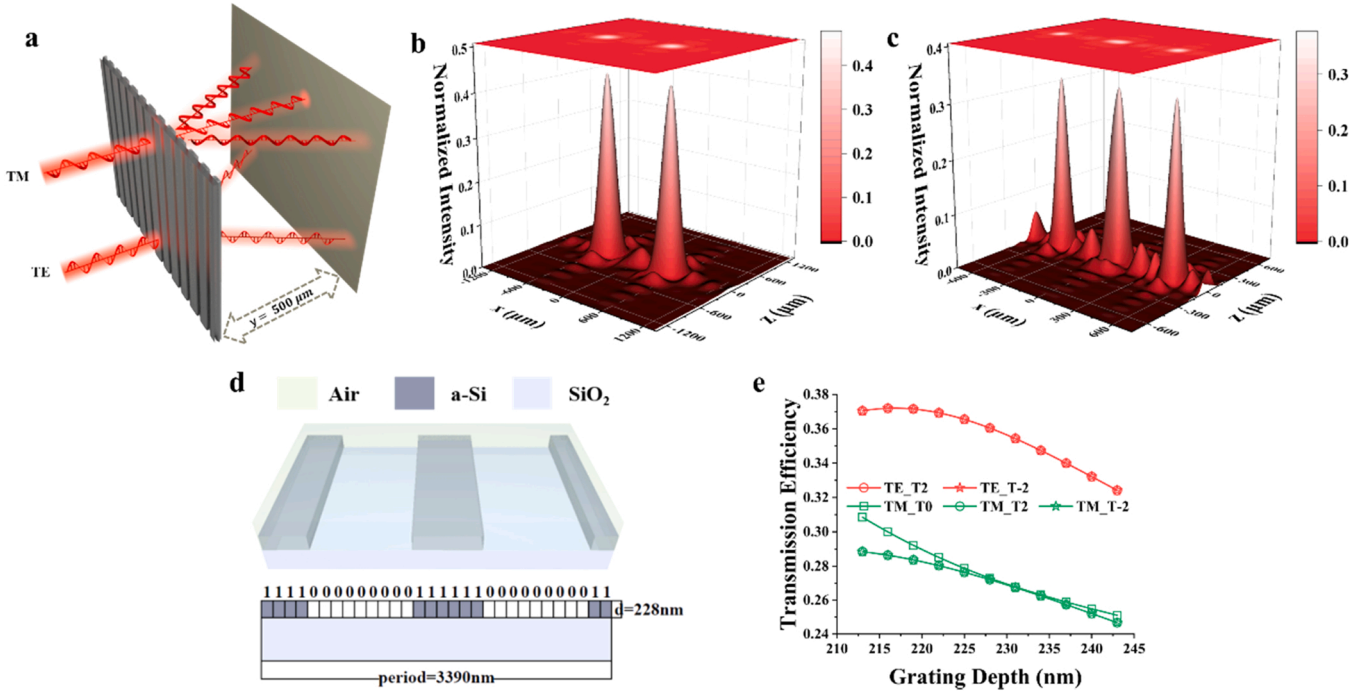

Fig. 2. Transmissive near-infrared laser beam splitter. (a) Schematic of multifunctional laser beam splitter. The incident beam is splitted into two energy-equal beams for TE polarization, while it is splitted into three for TM polarization. (b) Far-field electric intensity distributions of the splitted beams for TE incidence. (c) Far-field electric intensity distributions of the splitted beams for TM incidence. (d) The layer structure and the binary sequence of inversely designed supercell metagratings. The material of grating ridge is $_{Si}$, and the substrate is SiO_2. The light is normally incident from the substrate side of the beam splitter. (e) Transmission efficiency as functions of grating depths. T0, T2, T-2 indicate the zero-, 2nd, and − 2nd order of transmitted waves.

polarization, three orders (0, ± 2) of the diffracted light are remained after passing through the same beam splitters, as shown in Fig. 2(c). Fig. 2(d) provides the details of one-byte structure of designed supercell gratings. The optimized parameters are: grating depth 228 nm, the 'bit' resolution 113 nm and the 'byte' dimension 30. The data structure of a 'byte', that is the binary sequence, is depicted in the bottom part of Fig. 2 (d). In addition, we test the robustness of such a metagrating subjecting to potential fabrication errors. Fig. 2(e) shows the diffraction efficiencies as a function of grating depth error. For the TE polarization, when the depth varies ± 7.5%, the energy uniformity remains perfect although the transmission efficiency slightly decreases (< 5 %). For the TM polarization, equal energy can be also achieved between ± 2 orders of the diffracted beams for the same fabrication error. If the 0 order is further considered, the depth tolerance is reduced to ± 2 %.

Now, more complicated functions of the beam splitter are further considered here: 1) The wavelength window is shifted to the visible regime; 2) A broadband of wavelength is covered; 3) TE-polarized beam is equally splitted while the TM-polarized can go through the metagrating without bending. Fig. 3(a) illustrates the basic functionality of such broadband beam splitter. As before, the light is normally incident in the air from the substrate side of the beam splitter. The incident light is splitted into two energy-equal TE-polarized beams and one TM-polarized beam. The sum energy of TE components is expected to be equal to the energy of TM component. Fig. 3(b) shows the details of inversely designed structure. The ridge material of the metagrating is chosen as TiO_2 and the substrate is made of SiO_2 substrate. The optimized parameters are: grating depth 306 nm, the 'bit' resolution 57 nm and the 'byte' dimension 18. The data structure of a 'byte' is depicted in the bottom part of Fig. 3(b). The wavelength-dependent far-field (500 μm away from the beam splitter) electric intensity for the TE and TM components of the splitted beams can be seen from Fig. 3(c) and Fig. 3(d), respectively. The TE component is dominated by ± 1 diffraction orders, while the TM component is dominated by 0 diffraction order. As also can be seen from Fig. 3(c), the bending angle slightly alters with the wavelength, that is it increases from 29° to 36° when the wavelength varies from 500 nm to 600 nm. The average electric field intensity of each TE component remains high around 0.427, and the total average transmittance reaches 0.894 for TE polarization. As shown in Fig. 3(d), both the intensity and the propagation direction of the TM component are almost immune to the wavelength.

As a reverse process, optical beam merging is widely used in laser technology, combining energy of relatively lower power laser arrays to build high-power, good-beam-quality laser systems [43]. Without losing the generality, since we have shown two examples of transmissive metagrating devices, in the following we show how to design a reflective beam combiner in TM-mode by using the supercell metagrating concept and the same inverse design framework. Fig. 4(a) depicts the basic functionality of the optical beam combiner. Our goal is to merge the two beams with the incident angle of ± 45° into one, which is expected to reflect backward in a direction normal to the beam combiner. To achieve

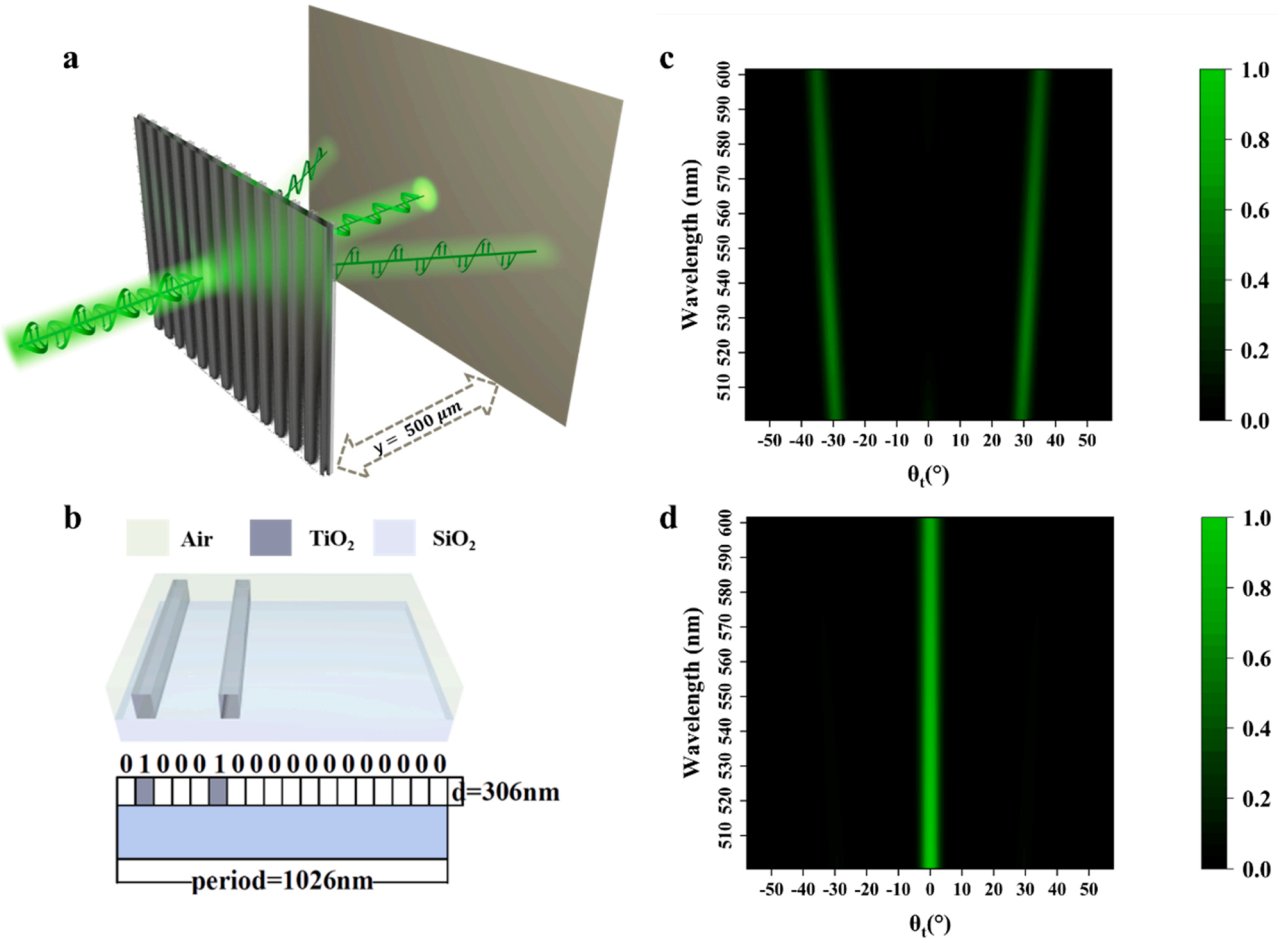

Fig. 3. Transmissive broadband beam splitter working in the visible regime. (a) Schematic diagram of polarization-dependent beam splitter by using the supercell metagrating. The incident light is splitted into two energy-equal TE-polarized beams and one TM-polarized beam. (b) The layer structure and the binary sequence of inversely designed supercell metagratings. The material of the grating ridge is TiO_2, and the substrate is SiO_2. The light is normally incident from the substrate side of the beam splitter. (c) Wavelength-dependent far-field electric intensities and the bending angles of TE components. (d) Wavelength-dependent far-field electric intensity and the bending angle of TM component.

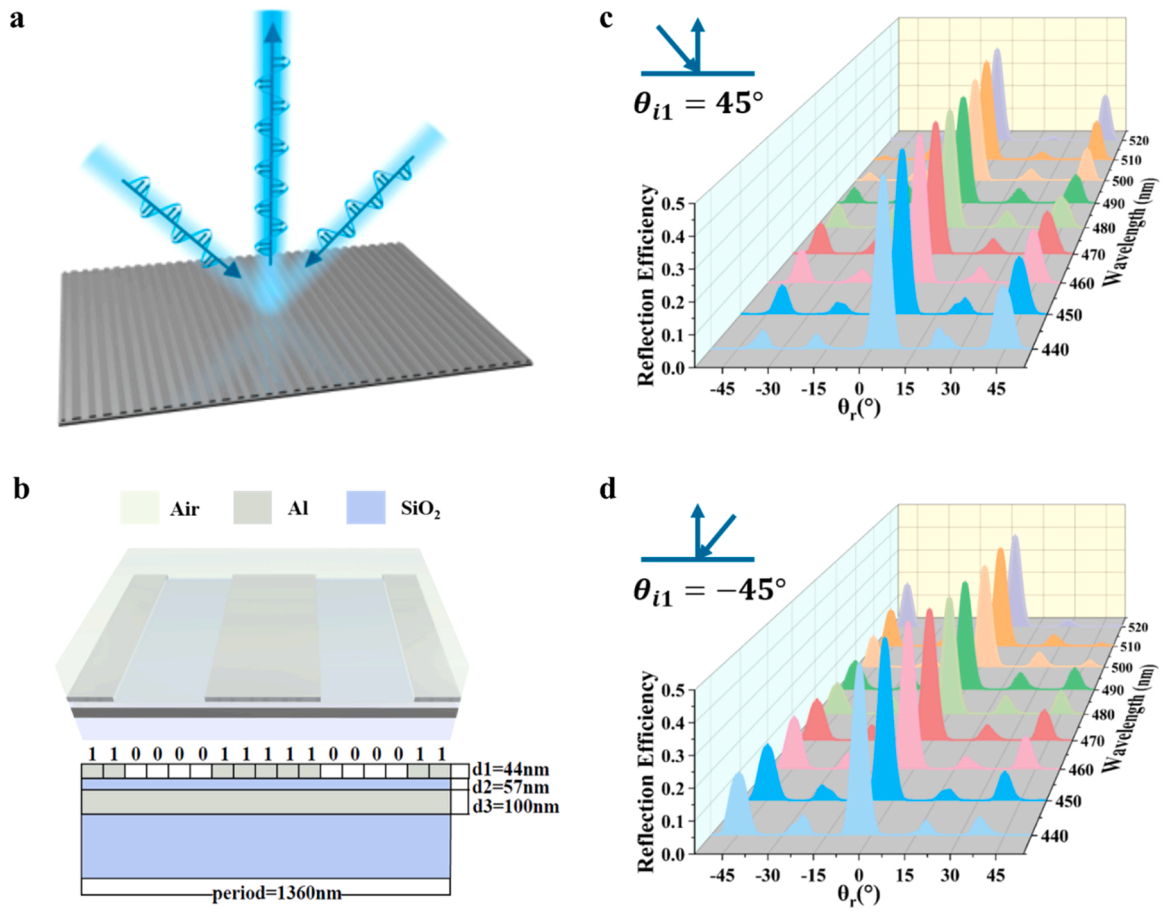

Fig. 4. Reflective broadband optical beam combiner working in the visible regime. (a) Schematic diagram of a beam combiner by using the metagrating. Two beams with the incident angles of ± 45° are merged to a vertically reflective beam. (b) The layer structure and the binary sequence of inversely designed supercell metagratings. The material of the grating ridge is Al. A 100 nm thickness of Al layer is sandwiched by the SiO_2 substrate and a 57 nm of SiO_2 layer. The light is incident from the air. (c) Far-field electric intensities of different reflection orders of a laser beam with the incident angle of 45°. The wavelength of the incident beam ranges from 440 nm to 520 nm. (d) Far-field electric intensities of different reflection orders of a laser beam with the incident angle of − 45°. The wavelength of the incident beam ranges from 440 nm to 520 nm.

a high reflection efficiency, a 100 nm of Al layer is sandwiched by the SiO_2 substrate and a 57 nm of SiO_2 layer. The SiO_2 layer can be deposited over the Al layer by using plasma-enhanced chemical vapor deposition in the experiment. The incident wavelength ranges from 440 nm to 520 nm. As shown in Fig. 4(b), the grating material we choose is Al, because of less interband transition induced absorption losses in comparison with Au and Ag [44,45]. The optimized parameters are: grating depth 44 nm, the 'bit' resolution 80 nm and the 'byte' dimension 17. The data structure of a 'byte' is depicted in the bottom part of Fig. 4 (b). For the beam with incident angle of 45°, the dominant diffraction order is − 2, the reflection angle of which is 0, as shown in Fig. 4(c). The dominant mode generally occupies more than 67.9% of the total reflection energy, while the zero order is depressed less than 9.2% for central wavelength in such a design. The same conclusions can be made for the beam with the incident angle of − 45°, owing to the rotation symmetry along the normal of grating plane, as calculated in Fig. 4(d).

4. Experimental demonstrations

To verify the performances of supercell metagratings and our computational framework, a multifunctional laser beam splitter shown in Fig. 2 is fabricated, following the standard planar technologies (see the details from 'Supplemental Documents'). Fig. 5(a) shows a scanning electron microscopy image of a unit cell of fabricated supercell metagrating. The sample is then put into a collimated optical path and the output beams are viewed with the assistance of an infrared detector card (Thorlabs, VRC2). The incident wavelength of the tunable laser we employed can be tuned from 1260 nm to 1300 nm (see the details from 'Supplemental Documents'). Fig. 5(b) shows the optical images and the power distributions of the splitted beams on the detector card. The laser wavelength is 1260 nm. The error bars indicate the averaged levels repeated for 5 times for each measurement. Even the optimal wavelength is designed at 1240 nm, the beam splitter working at 1260 nm exhibits comparable performances. As can be clearly observed from Fig. 5(b), two and three energy-equal beams are obtained from TE and TM polarized light, respectively. The sum energy of TE components (0.71) is approximately equal to the sum energy of TM components (0.74). These results unambiguously validate our proposed model system. To further test the wavelength compacity, the laser wavelength is tuned from 1260 nm to 1300 nm in a step of 10 nm. The transmissions of different diffraction orders for the TE and TM polarization are experimentally measured, as shown in Fig. 5(c). For the TE polarization, the energies of two separated beams are always equal and slightly increase with the wavelength. For the TM polarizations, the energies of three separated beams are almost equal. The energy deviation between the 0 order and ± 2 orders increases with the wavelength. Similar behaviors of diffraction efficiencies for the two polarization cases are predicted by the theoretical calculations, as shown in Fig. 5(d). Despite of slight differences on the absolute values, the transmission efficiencies show similar tendencies as the measurements. In particular, the slight energy deviation between the 0 order and ± 2 orders at the wavelength of 1260 nm shown in Fig. 5(c) has been predicted by theoretical

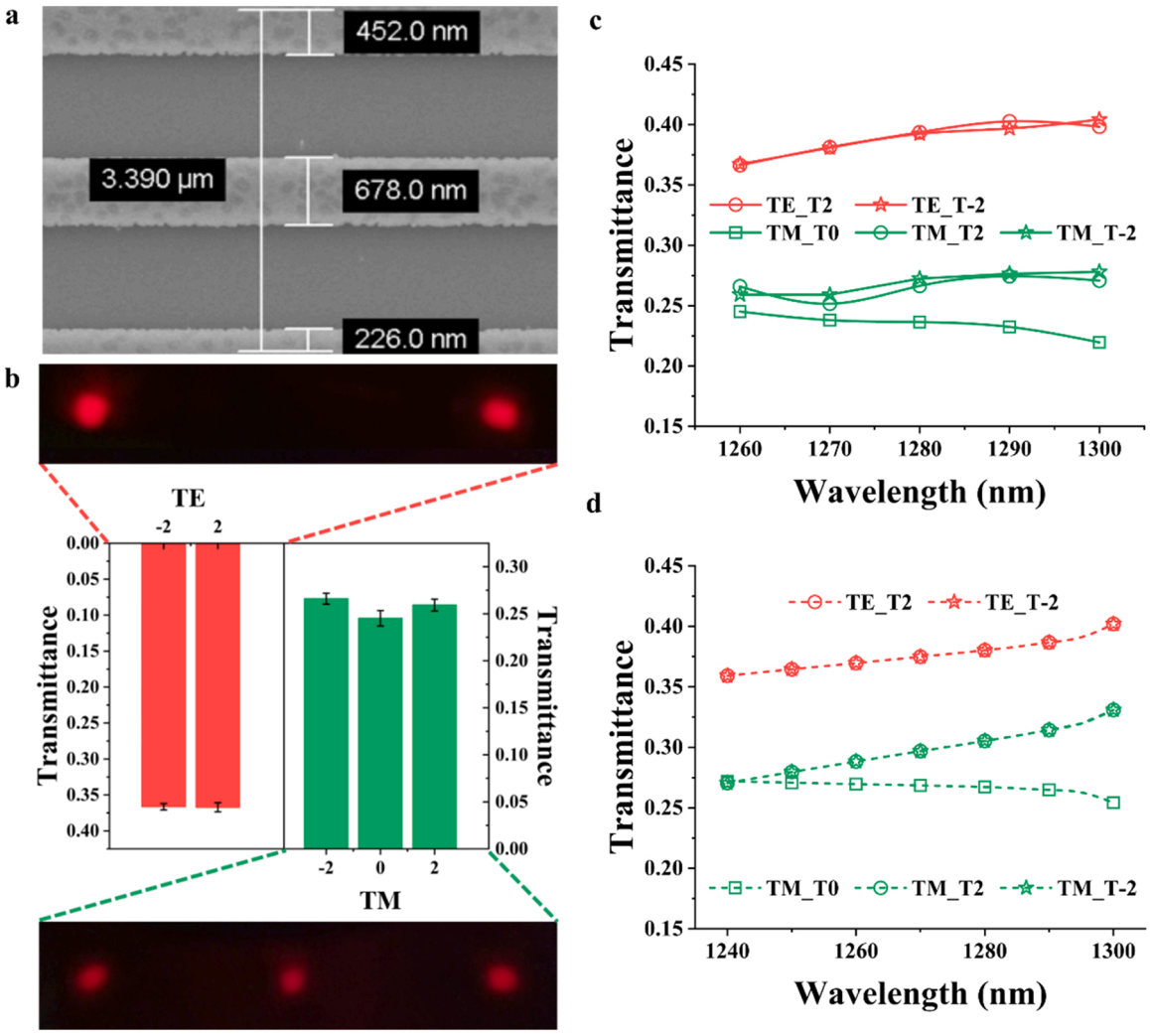

Fig. 5. Experimental demonstration of inversely designed transmissive near-infrared laser beam splitter. (a) Scanning electron microscopy image of the fabricated laser beam splitter. (b) The optical images and the power distributions of the splitted beams on the detector card. The laser wavelength is 1260 nm. The error bars indicate the averaged levels repeated for 5 times for each measurement. (c) Measured transmittance of splitted beams as functions of incident wavelength. (d) Calculated transmission efficiencies of splitted beams as functions of incident wavelength.

calculation as well. The deviation will disappear when the wavelength approaches 1240 nm.

5. Conclusions

In summary, we introduce the concept of supercell metagratings to the design of various optical beam routers. Instead of using two-dimensional periodic arrays, supercell gratings repeat the unit cells in one-dimension and thus greatly reduce the computational and nano-fabrication resources. Also, instead of using 'effective index-phase gradient' method, we use expanded coupled wave method as an electromagnetic solver and inverse design algorithms for the parameter optimization. By manipulating the digital structures of supercell unit cells, desired diffraction orders are strengthened while others are eliminated. The optical beam routers including two beam splitters and one beam combiner working in both visible and near-infrared regimes are rationally designed. Their polarization dependences and their energy distributions of desired orders can be quantitatively tailored. A broadband beam splitter is fabricated and experimentally validates our method. The work enriches the concept of flat optics, and pushes one step forward to the practical applications and mass production of the metagratings and metasurfaces.

Funding

The authors gratefully acknowledge the support from the National Natural Science Foundation of China (61927820, 51806199, 61905200) and the National Key Research and Development Program of China (2017YFA0205700).

Declaration of Competing Interest

The authors declare that they have no known competing financial interests or personal relationships that could have appeared to influence the work reported in this paper.

Data Availability

Data will be made available on request.

Appendix A. Supporting information

Supplementary data associated with this article can be found in the online version at doi:10.1016/j.photonics.2022.101075.

References

[1] U. Efron, Spatial Light Modulator Technology: Materials, Devices, and Applications, Marcel Dekker, 1995.
[2] R.A. Shelby, D.R. Smith, S. Schultz, Experimental verification of a negative index of refraction, Science 292 (5514) (2001) 77–79.
[3] D. Schurig, J.J. Mock, B.J. Justice, S.A. Cummer, J.B. Pendry, A.F. Starr, D. R. Smith, Metamaterial electromagnetic cloak at microwave frequencies, Science 314 (5801) (2006) 977–980.
[4] N. Yu, F. Capasso, Flat optics with designer metasurfaces, Nat. Mater. 13 (2) (2014) 139–150.
[5] J. Wang, A. Coillet, O. Demichel, Z. Wang, D. Rego, A. Bouhelier, P. Grelu, B. Cluzel, Saturable plasmonic metasurfaces for laser mode locking, Light: Sci. Appl. 9 (1) (2020) 1–9.
[6] F. Aieta, M.A. Kats, P. Genevet, F. Capasso, Multiwavelength achromatic metasurfaces by dispersive phase compensation, Science 347 (6228) (2015) 1342–1345.
[7] Y. Zhao, A. Alù, Manipulating light polarization with ultrathin plasmonic metasurfaces, Phys. Rev. B 84 (20) (2011), 205428.
[8] N. Yu, F. Aieta, P. Genevet, M.A. Kats, Z. Gaburro, F. Capasso, A broadband, background-free quarter-wave plate based on plasmonic metasurfaces, Nano Lett. 12 (12) (2012) 6328–6333.
[9] G. Zheng, H. Mühlenbernd, M. Kenney, G. Li, T. Zentgraf, S. Zhang, Metasurface holograms reaching 80% efficiency, Nat. Nanotechnol. 10 (4) (2015) 308–312.
[10] Y.-W. Huang, W.T. Chen, W.-Y. Tsai, P.C. Wu, C.-M. Wang, G. Sun, D.P. Tsai, Aluminum plasmonic multicolor meta-hologram, Nano Lett. 15 (5) (2015) 3122–3127.
[11] L. Wang, S. Kruk, H. Tang, T. Li, I. Kravchenko, D.N. Neshev, Y.S. Kivshar, Grayscale transparent metasurface holograms, Optica 3 (12) (2016) 1504–1505.
[12] L. Zhang, H. Zhang, N. Tang, X. Chen, F. Liu, X. Sun, H. Yu, X. Sun, Q. Jia, B. Chen, B. Cluzel, P. Grelu, A. Coillet, F. Qiu, L. Ying, W.E. Sha, X. Liu, J. Qiu, D. Zhao, M. Qiu, Plug-Play plasmonic metafibers for ultrafast fiberlasers, Light.: Adv. Manuf. 3 (2022) 45.
[13] L.-J. Yang, S. Sun, W.E.I. Sha, Z. Huang, J. Hu, Arbitrary vortex beam synthesis with donut-shaped metasurface, IEEE Trans. Antennas Propag. 70 (1) (2022) 573–584.
[14] S.S.A. Yuan, J. Wu, M.L.N. Chen, Z. Lan, L. Zhang, S. Sun, Z. Huang, X. Chen, S. Zheng, L.J. Jiang, X. Zhang, W.E.I. Sha, Approaching the fundamental limit of orbital-angular-momentum multiplexing through a hologram metasurface, Phys. Rev. Appl. 16 (6) (2021), 064042.
[15] Z.L. Deng, J. Deng, X. Zhuang, S. Wang, T. Shi, G.P. Wang, Y. Wang, J. Xu, Y. Cao, X. Wang, X. Cheng, G. Li, X. Li, Facile metagrating holograms with broadband and extreme angle tolerance, Light: Sci. Appl. 7 (2018) 78.
[16] Z.L. Deng, F.J. Li, H. Li, X. Li, A. Alù, Extreme diffraction control in metagratings leveraging bound states in the continuum and exceptional points, Laser Photonics Rev. 16 (6) (2022), 2100617.
[17] Y. Ra'di, D.L. Sounas, A. Alù, Metagratings: beyond the limits of graded metasurfaces for wave front control, Phys. Rev. Lett. 119 (6) (2017), 067404.
[18] Y. Fu, C. Shen, Y. Cao, L. Gao, H. Chen, C.T. Chan, S.A. Cummer, Y. Xu, Reversal of transmission and reflection based on acoustic metagratings with integer parity design, Nat. Commun. 10 (2019) 2326.
[19] D. Sell, J. Yang, S. Doshay, R. Yang, J.A. Fan, Large-angle, multifunctional metagratings based on freeform multimode geometries, Nano Lett. 17 (6) (2017) 3752–3757.
[20] E.R. Martins, J. Li, Y.K. Liu, J. Zhou, T.F. Krauss, Engineering gratings for light trapping in photovoltaics: the supercell concept, Phys. Rev. B 86 (4) (2012), 041404.
[21] T. Ye, D. Wu, Q. Wu, X.W. Sun, H. Liang, K. Wang, M. Hong, Realization of inversely designed metagrating for highly efficient large angle beam deflection, Opt. Express 30 (5) (2022) 7566–7579.
[22] Y. Xie, J. Quan, Q. Shi, Y. Cao, B. Sun, Y. Xu, Multi-functional high-efficiency light beam splitter based on metagrating, Opt. Express 30 (3) (2022) 4125–4132.
[23] Z. Wang, C. Dai, Z. Li, Z. Li, Free-space optical merging via meta-grating inverse-design, Nano Lett. 22 (5) (2022) 2059–2064.
[24] V. Popov, F. Boust, S.N. Burokur, Beamforming with metagratings at microwave frequencies: design procedure and experimental demonstration, IEEE Trans. Antennas Propag. 68 (3) (2020) 1533–1541.
[25] W. Wan, M. Luo, Y. Su, Ultrathin polarization-insensitive, broadband visible absorber based rectangular metagratings, Opt. Commun. 458 (2020), 124857.
[26] A. Karnieli, D. Roitman, M. Liebtrau, S. Tsesses, N.V. Nielen, I. Kaminer, A. Arie, A. Polman, Cylindrical metalens for generation and focusing of free-electron radiation, Nano Lett. 22 (14) (2022) 5641–5650.
[27] C. Hu, Y. Xu, S. Zhu, H. Chen, Phase-gradient metagratings via mode conversion, Phys. Rev. Appl. 17 (2) (2022), 024023.
[28] Y. Lu, H. Zou, J. Qian, Y. Wang, Y. Ge, S. Yuan, H. Sun, X. Liu, Multifunctional reflected lenses based on aperiodic acoustic metagratings, Appl. Phys. Lett. 119 (17) (2021), 173501.
[29] F. Uleman, V. Neder, A. Cordaro, A. Alù, A. Polman, Resonant metagratings for spectral and angular control of light for colored rooftop photovoltaics, ACS Appl. Energy Mater. 3 (4) (2020) 3150–3156.
[30] W. Liu, A.E. Miroshnichenko, Beam steering with dielectric metalattices, ACS Photonics 5 (5) (2017) 1733–1741.
[31] C. Spägele, M. Tamagnone, D. Kazakov, M. Ossiander, M. Piccardo, F. Capasso, Multifunctional wide-angle optics and lasing based on supercell metasurfaces, Nat. Commun. 12 (1) (2021) 1–10.
[32] D.J. Blumenthal, Photonic integration for UV to IR applications, APL Photonics 5 (2) (2020), 020903.
[33] P. Kaur, A. Boes, G. Ren, T.G. Nguyen, G. Roelkens, A. Mitchell, Hybrid and heterogeneous photonic integration, APL Photonics 6 (6) (2021), 061102.
[34] M.G. Moharam, T.K. Gaylord, E.B. Grann, D.A. Pommet, Formulation for stable and efficient implementation of the rigorous coupled-wave analysis of binary gratings, J. Opt. Soc. Am. A 12 (5) (1995) 1068–1076.
[35] M.G. Moharam, T.K. Gaylord, D.A. Pommet, E.B. Grann, Stable implementation of the rigorous coupled-wave analysis for surface-relief gratings: enhanced transmittance matrix approach, J. Opt. Soc. Am. A 12 (5) (1995) 1077–1086.
[36] P. Lalanne, G.M. Morris, Highly improved convergence of the coupled-wave method for TM polarization, J. Opt. Soc. Am. A 13 (4) (1996) 779–784.
[37] C. Wan, T.K. Gaylord, M.S. Bakir, Rigorous coupled-wave analysis equivalent-index-slab method for analyzing 3D angular misalignment in interlayer grating couplers, Appl. Opt. 55 (35) (2016) 10006.
[38] L. Li, Use of Fourier series in the analysis of discontinuous periodic structures, J. Opt. Soc. Am. A 13 (9) (1996) 1870–1876.
[39] L. Li, Note on the S-matrix propagation algorithm, J. Opt. Soc. Am. A 20 (4) (2003) 655–660.
[40] M.G. Moharam, T.K. Gaylord, Rigorous coupled-wave analysis of metallic surface-relief gratings, J. Opt. Soc. Am. A 3 (11) (1986) 1780–1787.
[41] J. Kennedy, R. Eberhart. Particle swarm optimization Proc. ICNN'95 - Int. Conf. Neural Netw., 4, 1995, pp. 1942–1948.
[42] J. Morio, Global and local sensitivity analysis methods for a physical system, Eur. J. Phys. 32 (6) (2011) 1577.
[43] T.Y. Fan, Laser beam combining for high-power, high-radiance sources, IEEE J. Sel. Top. Quantum Electron. 11 (3) (2005) 567–577.
[44] J. Wang, A.-L. Baudrion, J. Béal, A. Horneber, F. Tang, J. Butet, O.J. Martin, A. J. Meixner, P.-M. Adam, D. Zhang, Hot carrier-mediated avalanche multiphoton photoluminescence from coupled au–al nanoantennas, J. Chem. Phys. 154 (7) (2021), 074701.
[45] J. Wang, J. Butet, G.D. Bernasconi, A.-L. Baudrion, G. Lévêque, A. Horrer, A. Horneber, O.J. Martin, A.J. Meixner, M. Fleischer, P.-M. Adam, D. Zhang, Strong second-harmonic generation from au–al heterodimers, Nanoscale 11 (48) (2019) 23475–23481.